Singular robust room-temperature spin response from topological Dirac fermions

Lukas Zhao, Haiming Deng, Inna Korzhovska, Zhiyi Chen, Marcin Konczykowski, Andrzej Hruban, Vadim Oganesyan, Lia Krusin-Elbaum

▶ **To cite this version:**

Lukas Zhao, Haiming Deng, Inna Korzhovska, Zhiyi Chen, Marcin Konczykowski, et al.. Singular robust room-temperature spin response from topological Dirac fermions. Nature Materials, 2014, 13, pp.580. 10.1038/NMAT3962 . hal-00998601

HAL Id: hal-00998601

https://polytechnique.hal.science/hal-00998601

Submitted on 2 Jun 2014

HAL is a multi-disciplinary open access archive for the deposit and dissemination of scientific research documents, whether they are published or not. The documents may come from teaching and research institutions in France or abroad, or from public or private research centers.

L'archive ouverte pluridisciplinaire **HAL**, est destinée au dépôt et à la diffusion de documents scientifiques de niveau recherche, publiés ou non, émanant des établissements d'enseignement et de recherche français ou étrangers, des laboratoires publics ou privés.

Singular robust room-temperature spin response from topological Dirac fermions

Lukas Zhao,[1] Haiming Deng,[1] Inna Korzhovska,[1] Zhiyi Chen,[1] Marcin Konczykowski,[2] Andrzej Hruban,[3] Vadim Oganesyan,[4,5] & Lia Krusin-Elbaum[1]

[1]*Department of Physics, The City College of New York, CUNY, New York, NY 10031, USA & The Graduate Center, CUNY, New York, NY 10016, USA*

[2]*Laboratoire des Solides Irradiés, CNRS UMR 7642 & CEA-DSM-IRAMIS, Ecolé Polytechnique, F91128 Palaiseau cedex, France*

[3]*Institute of Electronic Materials Technology, 01-919 Warsaw, Poland*

[4]*Department of Engineering Science and Physics, College of Staten Island, CUNY, Staten Island, NY 10314, USA and*

[5]*The Graduate Center, CUNY, New York, NY 10016, USA*

Abstract

Topological insulators are a unique class of quantum solids where nontrivial inverted bulk band structure dictates the existence of metallic surface states[1–6] that are robust against impurity scattering[2,3]. This robustness is a consequence of the helical spin-momentum-locked nature[8–10] of the topological Dirac particles and is of great potential import, among other, to spin-based electronics[11]. In real three-dimensional (3D) topological insulators, however, the Dirac fermions intermix with the typically conducting bulk thereby complicating access to the low energy (Dirac point) charge transport or magnetic response. Here we use differential magnetometry to probe spin rotation in the 3D topological material family: Bi_2Se_3, Bi_2Te_3, and Sb_2Te_3. We report a discovery of a remarkable paramagnetic singularity in the magnetic susceptibility at low magnetic fields which persists up to room temperature, and which we demonstrate to arise from samples' surfaces. The singularity is universal to the entire topological family, largely independent of the bulk carrier density, and consistent with the existence of electronic states near the spin-degenerate Dirac point of the 2D helical metal. The exceptional thermal stability of the signal points to an intrinsic surface cooling process, likely of thermoelectric origin[12,13], and establishes a sustainable platform for the singular field-tunable Dirac spin response.

Enduring symbiosis between condensed matter physics and material science benefits whenever well established technological materials turn out to be remarkably good model systems for fundamentally new physical phenomena which in turn can lead to disruptive technological advances. Topological insulators are one recent example – prized thermoelectrics[12] since the 50's they also host topologically protected spin-helical surface states, as predicted by theory[1] (see Fig. 1a) and subsequently confirmed in a series of angularly resolved photoemission spectroscopy (ARPES) experiments[8,9,14]. Much of the activity since has been inspired by prospects of harvesting exotic properties of these helical states for electrical manipulation of magnetic memory[15] and error-free topological quantum computing[16].

Considerable effort is presently aimed at improving synthesis and characterization of these compounds with the goal of realizing materials with much suppressed bulk conduction channels – the latter tend to obscure surface physics, a problem particularly severe in charge transport[2,3]. Indeed, complex intermixing (hybridization) of the bulk and surface states is clearly observed by a variety of surface probes; for example recent time-resolved ARPES experiments reveal strong phonon-assisted surface-bulk coupling at high lattice temperature and unique cooling of Dirac fermions by acoustic phonons[13]. 'Aging' effects arising from complex surface reconstruction processes are also observed[17,18] – they tend to promote formation of 2D electron gas states of bulk origin in close proximity to the topological Dirac surfaces. Thus, existing materials continue to present a number of challenges to complete understanding of the physics of topological Dirac metal, especially at low frequencies and on mesoscales. Magnetic susceptibility measurements reported in this work witness singular magnetic response of topological surface states, but also hint at an intriguing cooling process involving these surface states and bulk carriers, thereby paving the way for systematic exploration of low energy electrodynamics of these transformative materials.

The experiments were performed using weak low frequency *ac* excitation field (see Fig. 1b and Methods) to probe linear response, focussing on its in-phase component, which is the equilibrium susceptibility $\chi(B) = \partial M(B)/\partial H$ in the limit of zero frequency and in a range of *dc* fields $B = \mu_0 H$, including the vicinity of $B = 0$ (see Supplementary Information, Section 1F). Figure 1c shows susceptibility of the canonical 2^{nd} generation topological insulator Bi_2Se_3 measured in *dc* fields $H \parallel c$-axis (normal to the $(00\bar{1})$ cleavage surface) of a platelike shaped crystal. Above $\sim 0.5\ T$ the response is diamagnetic, consistent with a decades old magnetic susceptibility measurements[19]. At lower fields, however, we detect a large cusplike *paramagnetic* susceptibility that sharply rises above the diamagnetic 'floor' in a narrow *dc* field range of ~ 0.2 T and approaching $\chi(H \to 0)$ in a straight line (Fig. 1c). This singu-

larity arises from sample's surface, is robust across all several topological samples measured and is most naturally ascribed to the opening of a Zeeman gap[3] at the Dirac point of the helical metal. Before we turn to substantiating these claims we note one particularly spectacular aspect to our data – its thermal stability. Indeed, the singular field dependence of the susceptibility shows no discernible signs of rounding up to the highest (room) temperature measured. This persistence of singular response to elevated temperature is remarkable and surprising when confronted with a rough conservative estimate of expected thermal smearing, *e.g.* obtained from the ratio of thermal energy at 300 K ($\simeq$ 27 meV) to the rather small bulk gap of these materials $\sim 100 - 300$ meV.

The presence of near-zero-field susceptibility cusp is universal – it is observed in all three topological insulators: Sb_2Te_3, Bi_2Te_3, and Bi_2Se_3 (Fig. 2a-2c). It is absent in all our calibration and background materials (see Supplementary Information Section C1, Fig. S3), which were carefully screened for any spurious signals. At higher fields, $H \gtrsim 0.5\ T$, the temperature-dependent diamagnetism dominates (Fig. 2d-2f, and Fig. S2); it appears to correlate with the details of the bulk band structure, but less clearly with the particulars of donor (n-type) or acceptor (p-type) intrinsic defects (Fig. 2g-2i) present in the bulk.

The height of the cusp is evidently sensitive somewhat to the density of defects quenched in during the crystal growth (see Methods), and there is an aging effect[18] that can reduce the height over time by an appreciable (up to 5) factor (an example is shown in Fig. S4). The cusp height in different crystals varies some with the intrinsic bulk carrier density, which in any particular crystal is determined from the measurements of Hall conductivity (see Fig. 2) or Shubnikov-de-Haas (SdH) quantum oscillations (Fig. S5). However the 'cuspiness' as quantified by the $B = \mu_0 H \to 0$ slope for any given member of this topological insulator family is universal. An example of this is shown in Fig. 3a, where we compare two Bi_2Te_3 crystals with carrier concentrations differing by two orders of magnitude. The cusp is frequency independent (Fig. 4a and Fig. S6), as expected for such low frequency response ($2 \sim 10$ kHz). And finally, the 'smoking-gun' evidence that the cusp is of the surface origin is illustrated in Fig. 3b, which shows that for the same crystal area, when the sample thickness is reduced the height of the cusp remains unchanged, while the diamagnetic background closely scales with the volume. We note that similar, albeit weaker, response is detected with the sample rotated by 90 degrees (see Fig. S1), consistent with the signal originating from noncleaving surfaces[20] where the Dirac dispersion is more complex.

Our finding of prominent singular magnetic response that survives high temperatures, huge variations in carrier density, and does not scale with sample volume is quite surprising and as

far as we know unprecedented. Absent any paramagnetic impurities (see Methods) or signs of itinerant ferromagnetism, the origin of this particular low field anomaly may be traced most naturally to the ungapped Dirac point. The simplest description of the Dirac fermions is captured by a non-interacting Rashba-type[21] Hamiltonian that effectively locks electron spin to its momentum, *i.e.* parallel to the sample's surface (see Supplemental Information, Sec. 2). Field applied transverse to the surface enters through a Zeeman coupling which we treat explicitly and via orbital quantization which we ignore (this approximation is justified by the absence of oscillatory effects at low fields in our experiments, and, *a posteriori*, we can also confirm that Dirac Landau level spacing is essentially negligible compared to the Zeeman gap in the parameter range relevant to our experiments – see Supplementary Information, Section 2). The equilibrium susceptibility is obtained by taking 2^{nd} derivative of the total free energy with respect to magnetic field B. With both chemical potential μ and temperature set to zero, low field *areal* (sheet) susceptibility χ_A (see Supplementary Information) reduces to

$$\chi_A(B) \cong \frac{(g\mu_B)^2\Lambda}{\hbar v_F} - \frac{2(g\mu_B)^3}{\hbar^2 v_F^2}|B| + \ldots, \tag{1}$$

where g is the Landé g-factor and v_F is the Fermi velocity. This paramagnetic Dirac susceptibility has a form of a cusp with a linear field decay at low fields, just as the cusp observed in our experiments (Fig. 3c). The maximum of χ_A depends on the effective size of the momentum space Λ contributing to the singular part of the free energy, and thus may be controlled in part by hexagonal warping of the Dirac cone[22] and by the details of the bulk bands. However, the singular *field dependence* only depends on universal (low energy) parameters through the slope $\frac{2(g\mu_B)^3}{\hbar^2 v_F^2}$ of χ in the limit $B \to 0$. To compare with the experiment we write the total susceptibility as a sum of the background contribution χ_0 and surface contribution $\chi = \chi_0 + \chi_A x/L_z$, where x is the fraction of the surface contributing and $L_z \approx 1\ mm$ is sample's thickness. We obtain a good match to the shape and the magnitude of the cusp (see Fig. 3c) by using parameter values consistent with the reported velocity v_F in Bi_2Te_3 from Landau level spectroscopy[23] and large effective g-factor[24], broadly consistent with the overall scale of g-factors expected for topological insulators and obtained from our SdH measurements (Figs. 3c and S5). The participating surface fraction that emerges from this analysis is remarkably small, $x \approx 0.002$, *i.e.* these states are very rare.

The existence of the sharp nonanalytic paramagnetic cusp at zero temperature requires the surface Fermi level to be at the Dirac point, $\mu = 0$. Otherwise, for $\mu \neq 0$, we expect a smooth dependence (rounding) near $B = 0$ with sharp jump singularities in χ on a field scale $\delta B = \mu/(g\mu_B)$ where the Fermi level enters the valence or conduction band.

Further phenomenological description can be facilitated by recastingthe low field paramagnetic response in Eq. 1 in terms of effective Dirac bandwidth $W = \hbar v_F \Lambda$ and field energy $E_B = g\mu_B B$ as $\chi_A(B) = \frac{(g\mu_B)^2\Lambda^2}{W}\left(1 - \frac{2E_B}{W} + \ldots\right)$, so the characteristic width of the cusp is set by the condition $W \approx E_B$. The observed temperature insensitivity requires thermal energy $E_T = k_B T \ll E_B < W$, or $T \lesssim 10K$, which may be relaxed somewhat on the level of this simple phenomenology if both g-factor and Fermi velocity are temperature dependent (Supplementary Information, Section 2).

In our experiments, no appreciable rounding of the cusp is observed – this finding is profoundly unexpected in view of the location of Fermi level gleaned from ARPES. Separate experimental work will be required to obtain a clear and detailed understanding of the microscopic origins of the electronic states giving rise to the singular response. From the established surface nature and the observed aging effects we infer that renormalization of the effective potential near the sample's surface in the course of aging is important. Also, the remarkable robustness to the variation in bulk carrier density and therefore bulk screening length, suggests that electrostatic models invoking bulk dopants as the dominant source of disorder at the surface may not be adequate to capture these states. Such models do readily produce large scale inhomogeneity of chemical potential, μ, which has been observed, for example, in graphene[25] and has been recently directly mapped in several topological insulators via scanning tunneling microscopy (STM)[26]. The typical amplitude of inhomogeneity in the latter study, $10 \sim 20$ meV, appears too small to couple to the electronic states near the Dirac point. However, rare states, that based on our analysis occupy only $\approx 0.2\%$ of sample's surface, may not be readily observed in STM. Moreover, the role played by unavoidable differences in surface preparation among different experiments remains to be established.

Yet more intriguing puzzle uncovered by our experiments is the apparent thermal stability of the singular response. This is certainly not within our simple Dirac phenomenology, which has in it scales on the order of only 10 K. In fact, we may argue that *any* equilibrium theory of the singular response in these narrowband semiconductors must show thermal effects near room temperature, as the band gap is only a few times larger, at best. We propose, therefore, that the local temperature at the location of electronic states responsible for the cusp is, in fact, strongly affected by the *ac* probe itself, *i.e.* these patches are kept at very low, possibly cryogenic effective temperature even though the cryostat and the rest of the sample are "warm". One plausible scenario (see Fig. 4) for this invokes disorder as the origin of local Peltier elements. The most natural source of power for the putative Peltier cooler is the rather large eddy current which does not contribute to χ itself but rather to the imaginary, out-of-

phase part of $\chi(\omega)$ (Fig. S7). To suppress Peltier heating (unavoidable due to *ac* excitation), this would require a rectifying element as well (see Fig. 4c and Fig. S9). From general consideration of the rectification process there should be then second harmonic generation, which we clearly observe (Fig. 4b). The above scenario implies strong enhancement of the effective (local) thermoelectric figure of merit as compared to known bulk values for these materials, which is quite natural, based on the existing work on improved thermoelectricity in nano-constrictions[27], and on strong frequency dependence of the transport coefficients under geometric confinement, as in the case of phonon heat conductivity[28]. We also note that strong (local) variations of material properties, *e.g.* due to the presence of disorder, can give rise to a novel variant of thermoelectric cooling, a "Thompson cooler", which has been predicted to display significant improvement of performance and, in principle, enable cooling to very low, even cryogenic temperatures[29]. Detailed theory of the mechanism of thermal stability is beyond the scope of this work and should be further explored.

Our experiments document a singularity in the low field response in a whole family of materials with topological surface states which does not arise from either strong correlations or fine tuning the chemical potential to the Dirac point. They are profoundly counterintuitive as they suggest the controlling role of rare states (patches) near the Dirac point realized under generic surface conditions in these samples. With this assumption we are able to reproduce the overall shape and magnitude of the response. One of the surprising quantitative insights that emerged was that a minority ($\lessapprox 0.2\%$) of the surface is responsible for the singular signal. This simple phenomenology is a step forward to a precise theoretical understanding and improved experimental control of these phenomena that will be crucial for manipulating robust polarization of protected surface states at room temperature.

Methods

Single crystals of Bi_2Se_3, Bi_2Te_3, and Sb_2Te_3 were grown by a modified Bridgman method (using evacuated quartz tubes in a horizontal gradient furnace heated to 1000^o C and cooled to room temperature in 7 days) or the standard Bridgman-Stockbarger method[23] using a vertical temperature gradient pull. The starting materials used in modified Bridgman were cm-sized chunks of Sb, Bi (purity of both 99.9999%), Te (purity 99.9995%), and Se (99.995%) from Alfa-Aesar used in stoichiometric ratios. X-ray diffraction of crystals was performed in Panalytical diffractometer using Cu Kα ($\lambda = 1.5405\mathring{A}$) line from Philips high intensity ceramic sealed tube (3 kW) X-ray source with a Soller slit (0.04 rad) incident and diffracted beam optics. The impurity level determined by elemental analysis using glow discharge mass spectrometry was found to be less than 0.005 ppm wt. We

used a series of crystals with different carrier densities (set by the number of charged vacancies and antisites quenched in during the crystal growth) which were obtained by varying the speed (down to 2 mm/hr) of the pull or the gradient profile in a horizontal or vertical setup. Carrier densities were determined from the measurements of Hall resistivity and Shubnikov-de Haas oscillations (see Supplementary Information). Differential susceptibility measurements were performed in a Quantum Design PPMS system, in a compensated pickup-coil detection configuration (Fig. 1b) with the *ac* excitation and detection coils designed to align with the the direction of applied static field. The *ac* excitation field amplitude was set at 10^{-5} T in a frequency range up to 10 kHz. Measurements of the sample holder and starting materials showed no pathological behavior near zero *dc* field (Fig. S3a,b,c). The system was calibrated using paramagnetic Pd standard, see Fig. S3d. The field scans at different temperatures over a larger field range for the topological insulators in this study are shown in the Supplementary Information. Calculations were performed using Mathematica.

---

[1] Fu, L., Kane, C. L. & Mele, E. J. Topological insulators in three dimensions. *Phys. Rev. Lett.* **98**, 106803 (2007).

[2] Hasan, M. Z. & Kane, C. L. Topological insulators. *Rev. Mod. Phys.* **82**, 3045-3067 (2010).

[3] Qi, X.-L. & Zhang, S.-C. Topological insulators and superconductors. *Rev. Mod. Phys.* **83**, 1057-1110 (2011).

[4] Chen, Y. L., Analytis, J. G., Chu, J.-H., Liu, Z. K., Mo, S.-K., Qi, X. L., Zhang, H. J., Lu, D. H., Dai, X., Fang, Z., Zhang, S. C. Fisher, I. R., Hussain, Z. & Shen, Z.-X. Experimental realization of a three dimensional topological insulator. Bi_2Te_3, *Science* **325**, 178-181 (2009).

[5] Hsieh, D., Xia, Y., Qian, D., Wray, L., Meier, F., Dil, J. H., Osterwalder, J., Patthey, L., Fedorov, A. V., Lin, H., Bansil, A., Grauer, D., Hor, Y. S., Cava, R. J. & Hasan, M. Z. Observation of time-reversal-protected single-Dirac-cone topological-insulator states in Bi_2Te_3, and Sb_2Te_3. *Phys. Rev. Lett.* **103**, 146401 (2009).

[6] Zhang, H., Liu, C.-X., Qi, X.-L., Dai, X., Fang, Z. & Zhang, S.-C. Topological insulators in Bi_2Se_3, Bi_2Te_3, and Sb_2Te_3 with a single Dirac cone on the surface. *Nature Phys.* **5**, 438-442 (2009).

[7] Castro Neto, A. H., Guinea, F., Peres, N. M. R., Novoselov, K. S. & Geim, A. K. The electronic properties of graphene. *Rev. Mod. Phys.* **81**, 109-162 (2009).

[8] Hsieh, D., Xia, Y., Wray, L., Qian, D., Pal, A., Dil, J. H., Osterwalder, J., Meier, F., Bihlmayer, G., Kane, C. L., Hor, Y. S., Cava, R. J. & Hasan, M. Z. Observation of unconventional quantum

spin textures in topological insulators. *Science* **323**, 919-922 (2009).

[9] Roushan, P., Seo, J., Parker, C. V., Hor, Y. S., Hsieh, D., Qian, D., Richardella, A., Hasan, M. Z., Cava, R. J. & Yazdani, A. Topological surface states protected from backscattering by chiral spin texture. *Nature* **460**, 1106-1109 (2009).

[10] Yazyev, O. V., Moore, J. E. & Louie, S. G. Spin polarization and transport of surface states in the topological insulators Bi_2Se_3 and Bi_2Te_3 from first principles. *Phys. Rev. Lett.* **105**, 266806 (2010).

[11] Awschalom, D. D., Loss, D. & Samarth, N., (editors). *Semiconductor Spintronics and Quantum Computation* (Springer, 2002).

[12] Venkatasubramanian, R., Siivola, E., Colpitts, T. & O'Quinn, B. Thin-film thermoelectric devices with high room-temperature figures of merit. *Nature* **413**, 597-602 (2001).

[13] Wang, Y. H., Hsieh, D., Sie, E. J., Steinberg, H., Gardner, D. R., Lee, Y. S., Jarillo-Herrero, P. & Gedik, N. Measurement of intrinsic Dirac fermion cooling on the surface of the topological insulator Bi_2Se_3 using time-resolved and angle-resolved photoemission spectroscopy. *Phys. Rev. Lett.* **109**, 127401 (2012).

[14] Hsieh, D., Xia, Y., Qian, D., Wray, L., Dil, J. H., Meier, F., Osterwalder, J., Patthey, L., Checkelsky, J. G., Ong, N. P., Fedorov, A. V., Lin, H., Bansil, A., Grauer, D., Hor, Y. S., Cava, R. J. & Hasan, M. Z. A tunable topological insulator in the spin helical Dirac transport regime. *Nature* **460**, 1101-1105 (2009).

[15] Essin, A. M., Moore, J. E. & Vanderbilt, D. Magnetoelectric polarizability and axion electrodynamics in crystalline insulators. *Phys. Rev. Lett.* **102**, 146805 (2009).

[16] Fu, L. & Kane, C. L. Superconducting proximity effect and Majorana fermions at the surface of a topological insulator. *Phys. Rev. Lett.* **100**, 096407 (2008).

[17] He, X., Zhou, W., Wang, Z. Y., Zhang, Y. N., Shi, J., Wu, R. Q. & Yarmoff, J. A. Surface termination of cleaved Bi_2Se_3 investigated by low energy ion scattering. *Phys. Rev. Lett.* **110**, 156101 (2013).

[18] Bahramy, M. S., King, P. D. C., de la Torre, A., Chang, J., Shi, M., Patthey, L., Balakrishnan, G., Hofmann, Ph., Arita, R., Nagaosa, N. & Baumberger, F. Emergent quantum confinement at topological insulator surfaces. *Nature Comm.* **3**, 1159 (2012).

[19] Mansfield, R. The magnetic susceptibility of bismuth telluride. *Proc. Phys. Soc.* **74**, 599-603 (1959).

[20] Zhang, F., Kane, C. L. & Mele, E. J. Surface states of topological insulators. *Phys. Rev.* B **86**, 081303(R) (2012).

[21] Bychkov, Y. A. & Rashba, E. I. Oscillatory effects and the magnetic susceptibility of carriers in inversion layers. *J. Phys. Chem.* **17**, 6039-6045 (1984).

[22] Fu, L. Hexagonal warping effects in the surface states of the topological insulator Bi_2Te_3. *Phys. Rev. Lett.* **103**, 266801 (2009).

[23] Wołoś, A., Szyszko, S., Drabinska, A., Kaminska, M., Strzelecka, S. G., Hruban, A., Materna, A. & Piersa, M. Landau-level spectroscopy of relativistic fermions with low Fermi velocity in the Bi_2Te_3 three-dimensional topological insulator. *Phys. Rev. Lett.* **109**, 247604 (2012).

[24] Analytis, J. G., McDonald, R. D., Riggs, S. C., Chu, J.-H., Boebinger, G. S. & Fisher, I. R. Two-dimensional Dirac fermions in a topological insulator: transport in the quantum limit. *Nature Phys.* **6**, 960964 (2010).

[25] Martin, J., Akerman, N., Ulbricht, G., Lohmann, T., Smet, J. H., von Klitzing, K. & Yacoby, A. Observation of electron-hole puddles in graphene using a scanning single-electron transistor. *Nature Phys.* **4**, 144-148 (2008).

[26] Beidenkopf, H., Roushan, P., Seo, J., Gorman, L., Drozdov, I., Hor, Y. S., Cava, R. J. & Yazdani, A. Spatial fluctuations of helical Dirac fermions on the surface of topological insulators. *Nature Phys.* **7**, 939-943 (2010).

[27] Li, Y.-X. Thermopower in quasi-one-dimensional nano-constrictions with spin-orbit interaction. *Physics Lett.* A **358**, 7073 (2006).

[28] Sellitto, A., Alvarez, F. X. & Jou, D. Phonon-wall interactions and frequency-dependent thermal conductivity in nanowires. *J. Appl. Phys.* **109**, 064317 (2011).

[29] Snyder, G. J., Toberer, E. S., Khanna, R. & Seifert, W. Improved thermoelectric cooling based on the Thomson effect. *Phys. Rev.* **B** 86, 045202 (2012).

[30] Vazifeh, M. M. & Franz, M. Spin response of electrons on the surface of a topological insulator. *Phys. Rev.* B **86**, 045451 (2012).

Acknowledgements We greatly appreciate the insights of Kyunghwa Park and thank Gil Refael for his useful suggestions and comments. We gratefully acknowledge Glen Kowach for his generous help and expert advice with the Bridgman crystal growth and Agnieszka Wołoś for selecting crystals with low carrier density. This work was supported by the NSF DMR-1122594 (L.K.-E.) and DMR-0955714 (V.O.).

Author contributions Experiments were designed by L.Z. and L.K.-E.. L.Z. and H.D. carried out the growth of single crystals, M.K. and A.H. provided Bi_2Te_3 crystals with the lowest carrier densities, and I.K. and Z.C. performed structural and chemical characterization of all crystals. *ac*

susceptibility measurements were done by L.Z. and H.D., data analysis was done by L.Z. and L.K.-E. Dirac phenomenology and the mechanism of Peltier cooling were formulated jointly by V.O. and L.K.-E. L.K.-E. and V.O. wrote the manuscript with critical input from L.Z.

Additional information The authors declare that they have no competing financial interests. Supplementary information accompanies this paper on www.nature.com/naturematerials. Correspondence and requests for materials should be addressed to L. K.-E.

FIGURE LEGENDS

Figure 1 | Dirac point origin of the large singular spin susceptibility near zero magnetic field. a, The energy-momentum relation of the surface states in a 3D topological insulator has a spin-helical Dirac cone structure arising from strong spin-orbit interaction that locks spins to their momentum[14]. For the $(00\bar{1})$ surfaces parallel to the quintuple layers[2] of a layered topological insulator such as Bi_2Se_3 the spin texture near Dirac point is riding on a circular constant energy contours of the Dirac bands, with spins aligned along the normal to the momentum. At the Dirac point, however, electron spins should be free to align along the tiny field as long as the Dirac spectrum is not gapped. **b**, Magnetic susceptibility of Bi_2Se_3 measured by applying a small *ac* excitation field h_{ac} (see Methods) shows that **c**, spin response is cusp-like and large near zero applied *dc* magnetic field. The susceptibility cusp is remarkably robust up to room temperature for both, $H \parallel c$-axis and $H \parallel ab$ field directions, see Fig. S1. It rides on a temperature dependent diamagnetic background, see Fig. S2. Here, the data at different temperatures were shifted to the lowest temperature of this study to indicate that both the slope and the height of the cusp between 1.9 K and 300 K remain intact.

Figure 2 | Universality of singular spin response near zero magnetic field. The zero-field susceptibility cusp is found in all three topological insulators: **a**, Sb_2Te_3, **b**, Bi_2Te_3, and **c**, Bi_2Se_3. The susceptibility surface in the $H - T$ phase space for fields above $H \sim 0.5\ T$ is shown in **d**, for Sb_2Te_3, in **e**, for Bi_2Te_3, and in **f**, for Bi_2Se_3 (see Supplementary Information). The most pronounced temperature dependence is found in Sb_2Te_3 (**d**), which has the smallest bulk bandgap of ~ 100 meV. **g-i**, Corresponding schematic band structures[6] indicate noticeable differences in the location of the Dirac point relative to the bulk valence and conduction bands. Measurements of Hall resistivity (insets in **g-i**) show that Te-based TIs, Sb_2Te_3 and Bi_2Te_3, are intrinsically *p*-type, while the Se-based TI, Bi_2Se_3 is *n*-type.

Figure 3 | Signatures of the surface origin of the cusp. a, Susceptibility cusp for two Bi_2Te_3 crystals with carrier densities differing by two orders of magnitude. The slope of the cusp is independent of the bulk carrier density n. Here the diamagnetic background was subtracted and the height of the cusp was normalized to $\chi(B = 0)$, which for the $n \sim 10^{-19}$ cm^{-3} crystal was 3×10^{-5} emu/cc, and for the $n \sim 10^{-17}$ cm^{-3} crystal was 3.5×10^{-5} emu/cc. **b**, Left: Susceptibility cusp before and after cutting the crystal thickness by a factor of 0.63 (red), 0.29 (green), and 0.15 (blue) appears to be independent of thickness

t. The diamagnetic background scales with thickness (volume for the fixed sample area A). Right: The data for all thicknesses shown on the left shifted to match the diamagnetic background. The signal to noise decreases with sample volume. **c**, The simple Dirac model of Eq. 1 produces a very good match to the data, as illustrated for the case of Sb_2Te_3 (see also Supplemental Information). Here $\chi = x\chi_A/L_z$ and χ_A is the 2D susceptibility of the Dirac state, $L_z \approx 10^{-3}m$, thickness of our samples, and $x < 1$ the effective areal fraction occupied by the ungapped Dirac state (x is used as a fitting parameter). Other parameter values used to generate this plot are $\mu = k_BT = 0, g = 30, v_F = 3 \cdot 10^3 m/s$, which are known from our own studies (see Supplemental Information) and those of others[23]. Both x and Λ (effective radius of **k**-space contributing to singular response) were adjusted to match the data, producing $x \approx 0.033$ and $\Lambda = 2 \cdot 10^8 m^{-1}$. The cusp is preserved even when hexagonal warping (inset in **c**) is taken into account[22] – it is merely subsumed into Λ. **d**, Rare regions of chemical potential $\mu \approx 0$ (grey) can exist in-between electron (blue) and hole (yellow) droplets due in part to electrostatic potential established by the charged defects in the bulk[26]. Such fluctuations of the local surface charge are likely "healing" in the course of the aging process[17,18] as the mean chemical potential steadily floats *away* from the Dirac point towards bulk conduction or valence bands, as has been documented in ARPES studies[17,18]. This is qualitatively consistent with the observed decrease in the amplitude of the paramagnetic anomaly over time.

Figure 4 | Surface cooling by the bulk. a, The in-phase component of the susceptibility containing the singular cusp is frequency independent (shown here for Sb_2Te_3). However, the *diamagnetic* susceptibility is frequency dependent (see Fig. S6). **b**, The nonlinearity of the surface-bulk connection is witnessed by the observed 2^{nd} harmonic of χ. It is consistent with the existence of "rectifying" paths in the putative thermoelectric cooling elements (sketched in **c**, also see Figs. S8, S9 and Supplementary Information) required for the cooling of small fraction of sample's surface and thus suppressing thermalization of Dirac surfaces with the bulk, as explained in text. The effective cooling of the surface is naturally achieved by the electron and hole puddles in the sub-surface region forming a Peltier element owing its cooling efficiency partly to nanoconstriction and partly to frequency-dependent transport coefficients[28].

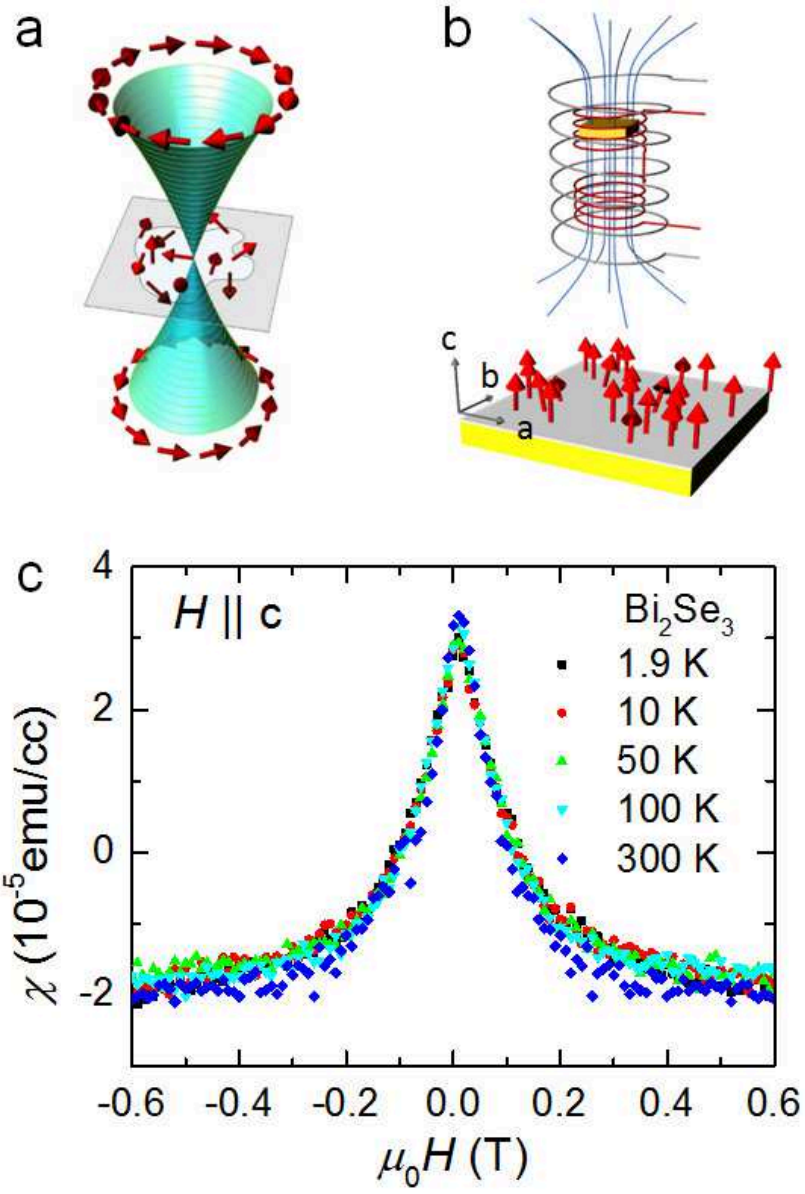

Fig. 1 Zhao *et al.*

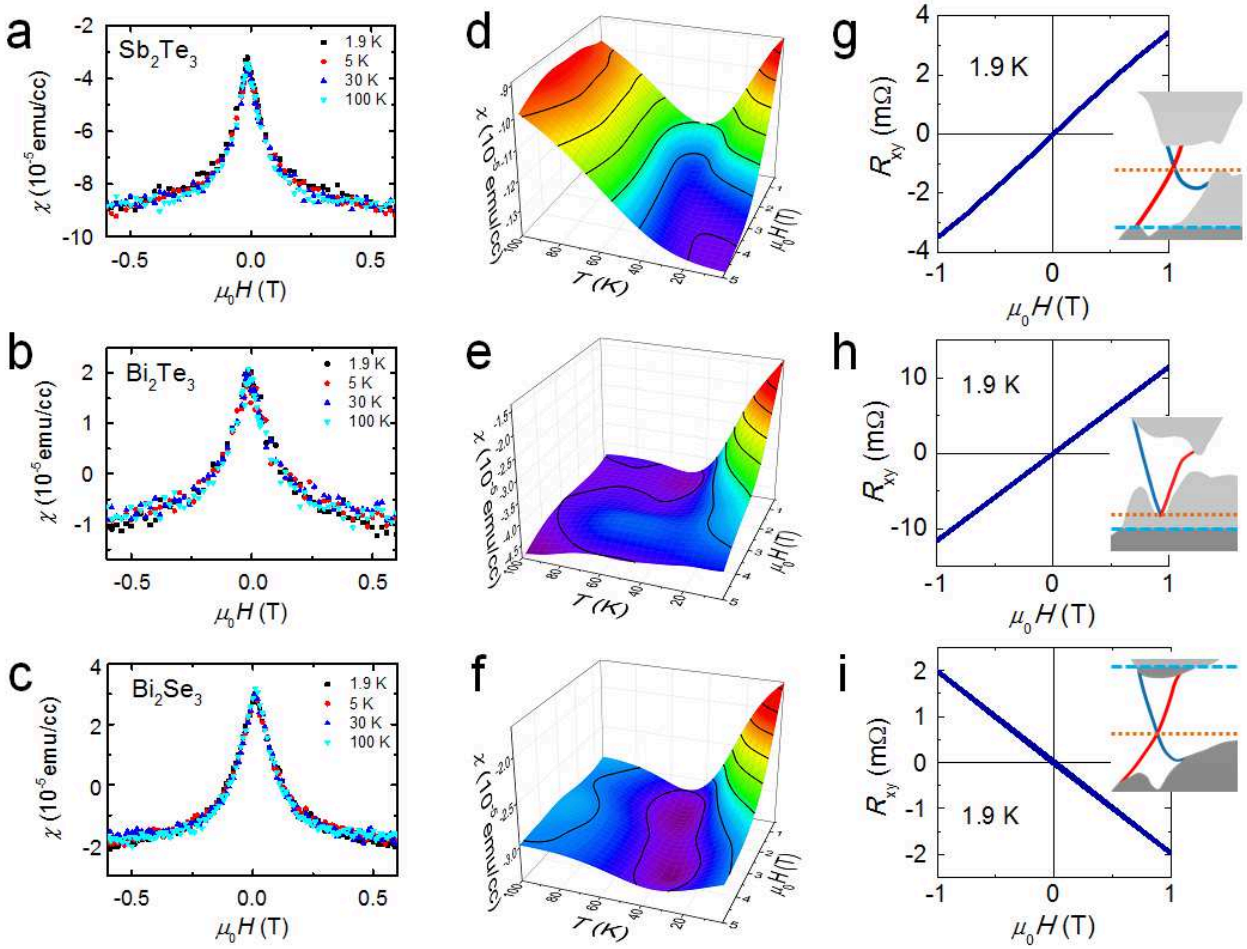

Fig. 2 Zhao *et al.*

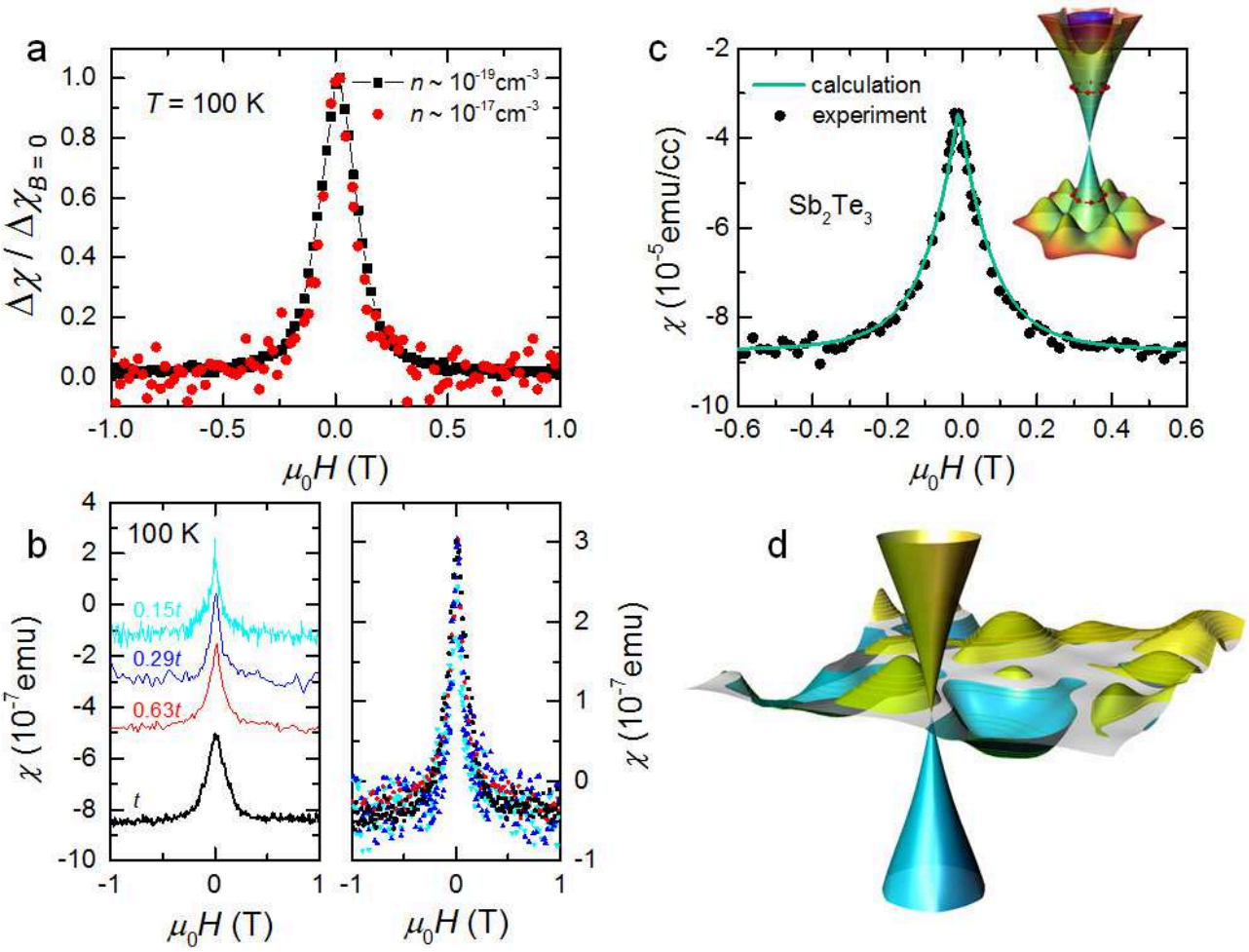

Fig. 3 Zhao *et al.*

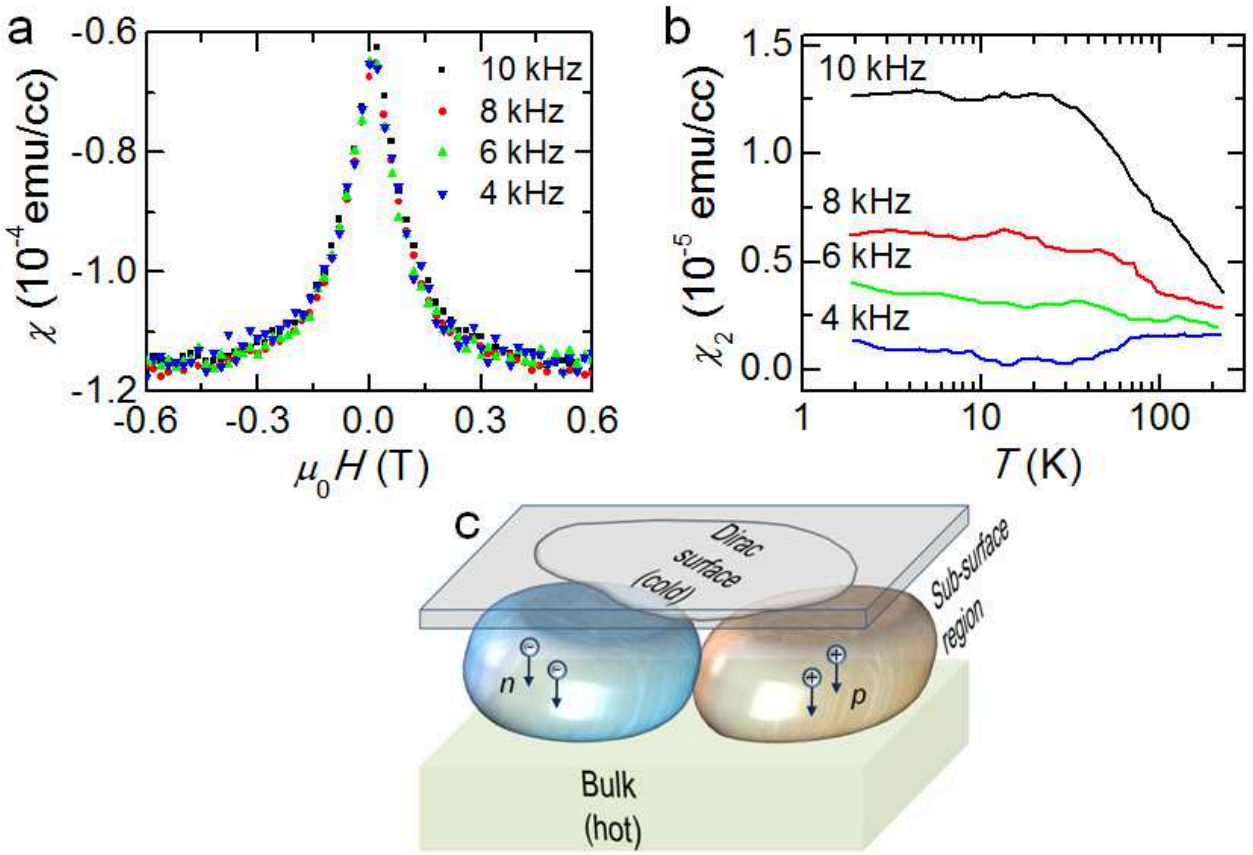

Fig. 4 Zhao *et al.*